Improved Output Performance of Direct-Current Triboelectric Nanogenerator through Field Enhancing Breakdown Effect

Shengyang Chen, Di Liu, Linglin Zhou, Shaoxin Li, Zhihao Zhao, Shengnan Cui, Yikui Gao, Yanhong Li, Zhong Lin Wang,* and Jie Wang*

The emerging direct-current triboelectric nanogenerator (DC-TENG) does not need to be rectified and is not restricted by a dielectric breakdown compared with an alternating current TENG (AC-TENG). Furthermore, the charge density of the DC-TENG reaches an ultrahigh level far beyond that of the AC-TENG based on a rational design. However, there are always some electrons remaining on the surface of the dielectric after the breakdown process in the DC-TENG, and therefore a low charge utilization is obtained. Herein, a simple and universal method is proposed through a double-layer structure design, that is, a triboelectric layer as the friction layer and an electret layer charged through a surface treatment as the field-enhancing layer to further improve the output performance of the DC-TENG, which is inspired by the fable "The Crow and the Pitcher." Owing to the external field-enhancing breakdown effect, a double improvement in the breakdown efficiency and output charge density is obtained compared with a conventional DC-TENG. Moreover, a nearly constant output current has been demonstrated for directly powering electronics without a rectifier. This study provides a universal method for optimizing the output performance of a DC-TENG.

1. Introduction

As the world enters the new era of Internet of Things, big data, and artificial intelligence, widely distributed sensor networks with the characteristics of a random distribution, enormous amounts of data, and mobile and wireless communications have led to an increased energy demand, and a constant current power supply is required to drive their continuous operation. It is extremely challenging to solve these formidable problems using batteries owing to the disadvantages of a limited lifespan, non-negligible maintenance costs, and in particular, environmental pollution. In recent years, ambient energy harvesting technologies have become a sustainable, clean, and promising strategy for the distribution of energy demand, and various types of generators have been developed based on different working mechanisms, such as solar cells, electromagnetic generators, thermoelectric generators, piezoelectric generators, and triboelectric nanogenerators (TENGs).[1] Among them, the conversion and utilization of mechanical energy are undoubtedly considered one of the most promising choices owing to its wide distribution and variety of forms. In 2012, the TENG was invented by Prof. Wang's group based on the coupling of contact electrification and electrostatic induction, and has been demonstrated as a promising strategy to convert random, distributed, and low-frequency mechanical energy into electric energy owing to the merits of a low cost, broad material selection, and diverse structural design.[2–6]

In general, the output characteristics of conventional TENGs are an alternating current (AC) and pulse,[7] which cannot drive electronic devices directly. To solve these problems, many studies have been proposed to produce a direct current (DC), which is mainly divided into two categories. One is utilizing the power management unit,[8,9] mechanical rectifier,[10,11] and phase control[12–15] to realize DC output and a low crest factor (the crest factor is defined as the ratio between the peak current and the root-mean square value), which may increase the complexity of the system and inevitably cause an energy loss. The other category is based on the "self-rectified" principles, such as a Schottky knot,[16,17] silicon p-n junction,[18,19] contact barrier between metal and semiconductor,[20]

S. Chen, Y. Gao, Y. Li, Prof. J. Wang
School of Physical Science and Technology
Center on Nanoenergy Research
Guangxi University
Nanning 530004, P. R. China
E-mail: wangjie@binn.cas.cn
S. Chen, D. Liu, Dr. L. Zhou, S. Li, Dr. Z. Zhao, S. Cui, Y. Gao, Y. Li,
Prof. Z. L. Wang, Prof. J. Wang
Beijing Institute of Nanoenergy and Nanosystems
Chinese Academy of Sciences
Beijing 100083, P. R. China
E-mail: zhong.wang@mse.gatech.edu
D. Liu, Dr. L. Zhou, S. Li, Dr. Z. Zhao, S. Cui,
Prof. Z. L. Wang, Prof. J. Wang
College of Nanoscience and Technology
University of Chinese Academy of Sciences
Beijing 100049, P. R. China
Prof. Z. L. Wang
School of Materials Science and Engineering
Georgia Institute of Technology
Atlanta, GA 30332, USA

tunneling effect in a metal-insulator-semiconductor structure, and air breakdown effect.[21–23] In particular, the proposed DC-TENG based on contact electrification and air breakdown effect can realize a nearly constant output current,[24] which can drive electronic devices directly. Furthermore, owing to its merits of a high output charge density, simpler structure, and no restriction by the dielectric breakdown,[25–27] a DC-TENG is considered a potential solution to overcome the limitation of the charge density in conventional AC-TENG, showing significant potential for the miniaturization of self-powered systems.

As an energy harvester, further improving the output performance of the DC-TENG, which depends highly on the surface charge density, is a crucial research direction for promoting its practical applications.[28] The limiting factors of the effective surface charge density of the DC-TENG ($\sigma_{DC-TENG}$) can be described as follows.

$$\sigma_{DC-TENG} = k \times \min\left(\sigma_{triboelectrification}, \sigma_{c, electrostatic\ breakdown}\right) \tag{1}$$

where k is determined by the electrode structure design, $\sigma_{triboelectrification}$ is the charge density of triboelectrification, and $\sigma_{c, electrostatic\ breakdown}$ is the charge collected by an electrostatic breakdown.[29] According to previous reports, some residual charges always occur on the surface of the dielectric layer during the electrostatic process; thus, the electrostatic breakdown efficiency (η) can be defined as follows.

$$\eta = \frac{\sigma_{c, electrostatic\ breakdown}}{\sigma_{triboelectrification}} \tag{2}$$

Based on Equations (1) and (2), $\sigma_{DC-TENG}$ can be described as follows.

$$\sigma_{DC-TENG} = k \times \eta \times \sigma_{triboelectrification} \tag{3}$$

Currently, many efforts have been devoted to improving $\sigma_{DC-TENG}$ by enhancing η through the optimization of the working conditions (including the atmosphere composition, temperature, and atmosphere pressure)[30,31] and increasing k through the microstructure design of the DC-TENG, where an ultrahigh value of ≈5.4 mC m^{-2} is realized. To further increase the surface charge density of the DC-TENG, a simple and universal strategy through the improvement of η, which can be realized under normal conditions without the requirement of a special gas environment or high temperature, is highly desired.[32]

In this study, an electric field enhanced DC-TENG (E-DC-TENG) is proposed to improve η and the output performance of a DC-TENG under atmospheric conditions by utilizing the field-enhancing breakdown effect. Compared with a conventional DC-TENG, the air breakdown process of an E-DC-TENG can be greatly enhanced, which results in a nearly doubled improvement in η as well as transferred charges and short-circuit current and open-circuit voltage outputs. Furthermore, a rotary E-DC-TENG was fabricated for practical application, and a nearly constant output current was obtained, which has been demonstrated to directly power electronics without any rectifier or energy storage unit.
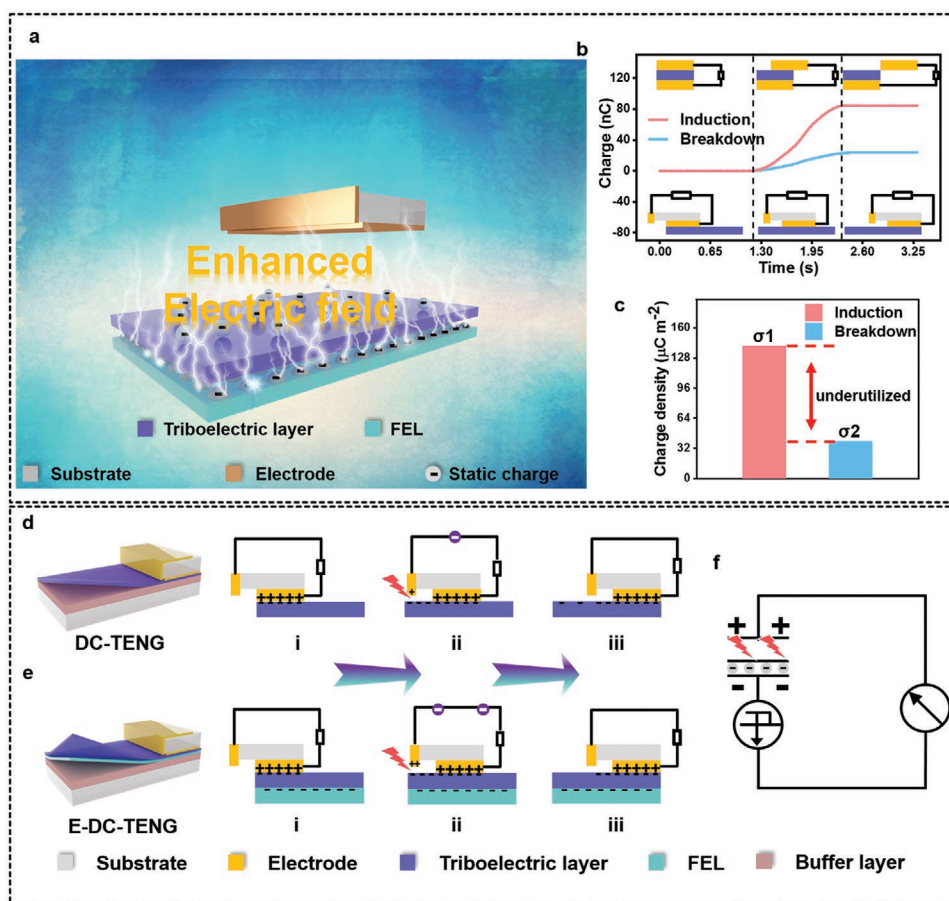
2. Results

2.1. Working Mechanism of E-DC-TENG for Improving the Breakdown Efficiency

The electric field enhancing the breakdown effect is introduced into a conventional DC-TENG to enhance the electric field intensity between the charge collecting electrode (CCE) and the charged triboelectric layer (PTFE) by adding a field enhancing layer (FEL), as described in Note S1, Supporting Information under the triboelectric layer. In this designed E-DC-TENG, the triboelectric layer and FEL play different roles. The former is the same as the dielectric layer in a conventional DC-TENG used for triboelectrification. The latter is used for applying a strong external electric field to enhance the electrostatic breakdown process, and more charges can then be collected from the CCE to realize an increase in the output performance of the DC-TENG, as shown in **Figure 1**a.

To quantitatively measure the charges existing on the surface of the dielectric layer after an air breakdown, which is the charge dissipation in DC-TENGs, a comparison between the charges from triboelectrification and an electrostatic breakdown is needed. As is well known, a conventional AC-TENG can be used as a simple method to measure the charges from triboelectrification through electrostatic induction,[33] whereas the output charges in the DC-TENG can be considered as the charges from the breakdown effect, as shown in Figure S1, Supporting Information. In general, the critical electric field for an air breakdown under standard atmospheric conditions is 3 kV mm^{-1}. In other words, there are always some charges on the surface of the dielectric layer after an air breakdown, resulting in a charge dissipation in the DC-TENG. A quantitative measurement of the output charges from the conventional sliding-mode AC-TENG and DC-TENG also confirms the charge dissipation, as shown in Figure 1b, where the effective area is 2 cm × 3 cm. We found that the transferred charge density in the DC-TENG is smaller than that of the conventional sliding-mode AC-TENG with the same sliding area, and the former is only ≈28% of the value in the latter, as shown in Figure 1c. Therefore, the goal of this study was to reduce the charges underutilized in a conventional DC-TENG.

We designed the sliding mode device to describe the working mechanisms of the conventional DC-TENG and E-DC-TENG in detail, as shown in Note S2, Supporting Information and Figure 1d,e, respectively. In stage I (the initial state), the frictional electrode (FE) is in contact with the dielectric layer (PTFE) and is aligned to the left of the PTFE; in addition, the charges are generated from the triboelectrification between the FE and PTFE with equally positive and negative charges distributed on their surfaces, respectively. As the slider continues to slide forward, a portion of the charges is then retained on the surface of the dielectric layer in the area where the FE has been rubbed, because PTFE is an electret material. There are also induced positive charges in the CCE, attributed to an electrostatic induction, and an electrostatic breakdown occurs across the air gap if the strong electric field is higher than 3 kV mm^{-1} (the voltage of air breakdown according to Paschen's law). It is worth noting that the electrostatic breakdown process is further enhanced owing to the external field formed by the FEL. A

**ADVANCED
SCIENCE NEWS**

www.advancedsciencenews.com

**ADVANCED
MATERIALS
TECHNOLOGIES**

www.advmattechnol.de

Figure 1. Working mechanism of the E-DC-TENG for improving the breakdown efficiency: a) Representative diagram of the E-DC-TENG. b) The transfer charges of electrostatic induction from AC-TENG and electrostatic breakdown from DC-TENG with the same sliding area. c) A comparison of charge density between electrostatic induction from AC-TENG and electrostatic breakdown from DC-TENG with the same sliding area in a cycle. d,e) Device diagram and illustration of working mechanism of sliding mode DC-TENG and E-DC-TENG. f) Equivalent circuit diagram of DC-TENG.
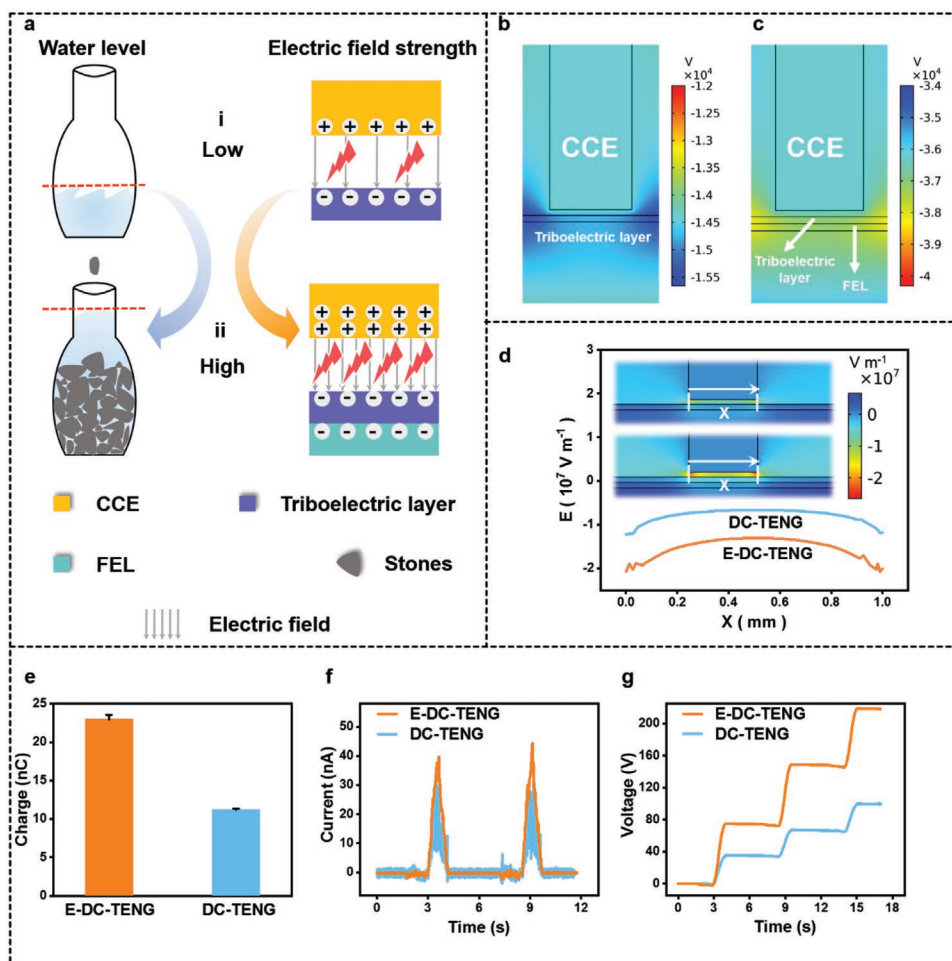
relatively low electrostatic field from the surface charge density (compared with the condition without an external electric field) combining the external electric field can easily reach the critical value for an air breakdown, and finally, more charges can be collected by the CCE. In stage III, the slider moves to the right margin of the dielectric layer, and the working cycle is finished. A more perspicuous equivalent circuit diagram of the E-DC-TENG is shown in Figure 1f, in which the charges arise from triboelectrification between the FE and the PTFE film, and then return to the CCE through an air breakdown, forming a closed loop in the external circuit.

2.2. Mechanism of Field Enhancing Breakdown Effect

The field-enhancing breakdown effect is inspired by the fable "The Crow and the Pitcher." To clearly illustrate the mechanism for optimizing the output performance of the DC-TENG, a specific model is proposed in **Figure 2**a. At the initial state shown in Figure 2a(i), the water level of the pitcher is far from the bottleneck and too low for the crow to drink from. As stones are placed into the bottle, the water level in the bottle rises, and thus becomes sufficiently high to drink. In general, the

negative electrostatic charges on the surface of the dielectric layer from triboelectrification will induce the same amount of positive charges in the CCE, and an electric field will then be built across the air gap, with the strength of the electric field remaining at a relatively low level. Similar to the ability of stones to increase the water level in E-DC-TENG, in addition to the electric field from triboelectrification, there is an additional electric field from the pre-charged dielectric layer, which is referred to as the FEL. Therefore, the electric field distribution across the air gap will be significantly enhanced, leading to a more violent breakdown, resulting in the charges on the surface of the dielectric layer more easily participating in the breakdown process, as shown in Figure 2a(ii).

The simulated results also confirmed the enhancement of the air breakdown process. The distributions of the potential across the air gap with and without the FEL are simulated in Figures 2b,c, respectively. The results indicate that the potential across the air gap in the E-DC-TENG is nearly double that of a conventional DC-TENG. In Figure 2d, the corresponding electric field strength distribution at the middle position of the air gap is plotted. It is clear that the maximum electric field strength in the DC-TENG is only $\approx -3 \times 10^7$ V m^{-1}, and a high electric field strength of $\approx -6 \times 10^7$ V m^{-1} appears in the

**ADVANCED
SCIENCE NEWS**

www.advancedsciencenews.com

**ADVANCED
MATERIALS
TECHNOLOGIES**

www.advmattechnol.de

Figure 2. The schematic mechanism of field enhancing breakdown effect. a) Schematic mechanism of field enhancing breakdown effect by adding FEL. b–d) Electric field distribution and the electric potential simulation between charge collection electrode and electrification in conventional DC-TENG and E-DC-TENG. e) Transferred charge in a cycle, and f) I_{sc} and g) V_{oc} outputs of conventional DC-TENG (blue line) and E-DC-TENG (yellow line).

E-DC-TENG, which indicates that the output charge of the E-DC-TENG may be twice that of the DC-TENG.

To further quantify the performance of the E-DC-TENG, we used a sliding-mode device. Before the electric output performance test, we used a simple method to demonstrate that the pre-modulated charges indeed exist on the FEL, and a detailed description is shown in Figure S2, Supporting Information. The output charge of the E-DC-TENG is 22 nC in one cycle, which is approximately twice that of the DC-TENG (11.5 nC at 0.4 Hz), as shown in Figure 2e. The breakdown efficiency "η" increased from 22.4% to 46% through the field-enhanced breakdown effect. This result is solid evidence demonstrating that the FEL can significantly improve the output performance of the DC-TENG. The corresponding short-circuit current (I_{sc}) and open-circuit voltage (V_{oc}) are shown in Figures 2f,g, respectively, with the same increasing tendency. To further prove its universality, the field-enhanced breakdown effect was also demonstrated using other triboelectric materials, such as fluorinated ethylene propylene and polyvinyl chloride, as shown in Figure S3, Supporting Information. Moreover, the specific model and theoretical simulation results not only verify the rationality of this method in principle, but also demonstrate its

uniqueness and universality for optimizing the output performance of the DC-TENG.

2.3. Output Performance of Sliding Mode E-DC-TENG

To clarify the performance of the E-DC-TENG and explore which parameters affect its output characteristics, we built an experimental device composed of a linear motor, a supporting plate, a weight, and an E-DC-TENG, as shown in **Figure 3**a. A linear motor was used to provide an external driving force for the linear motion of the slider. To ensure the same pressure during the entire experiment as much as possible, a weight of 200 g was placed on the E-DC-TENG to achieve stable pressure conditions. The transferred charges, I_{sc}, and V_{oc} of the sliding mode E-DC-TENG during one cycle at different accelerations are shown in Figures 3b–d, the effective area of which is 2 cm × 2 cm. The device model and detailed data of the sliding-mode DC-TENG and E-DC-TENG under the same conditions are shown in Figure S4, Supporting Information. With acceleration increases from 0.4 to 4 m s^{-2}, the amount of transferred charges remains almost constant because the amount of transferred charges is
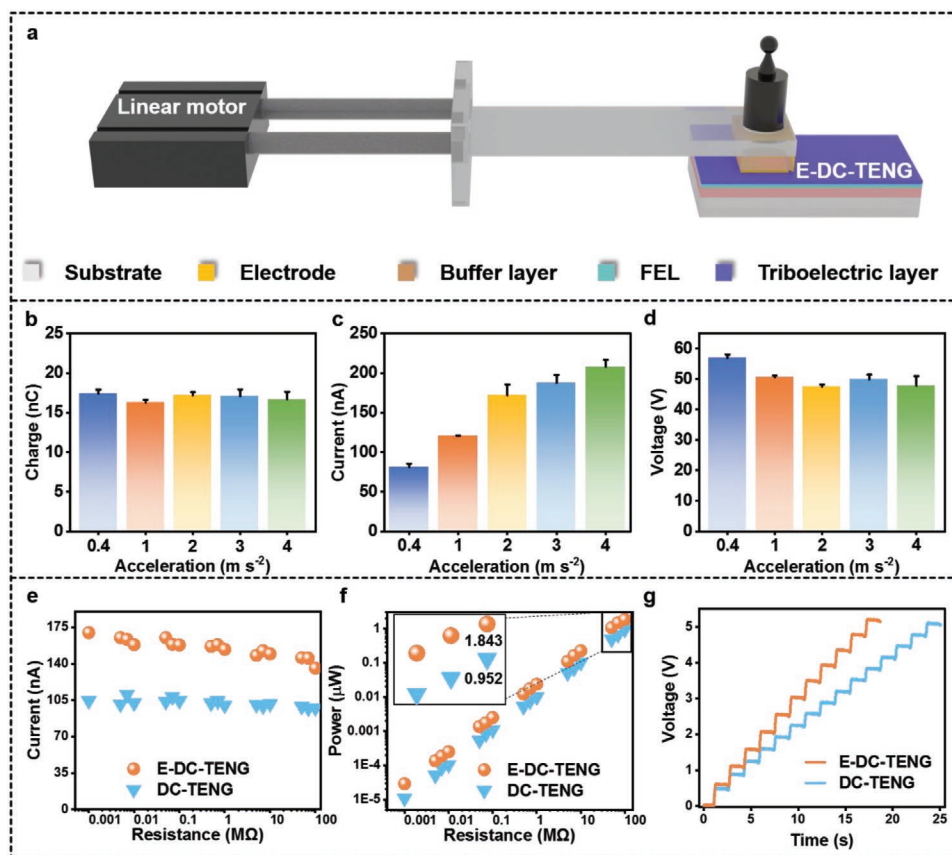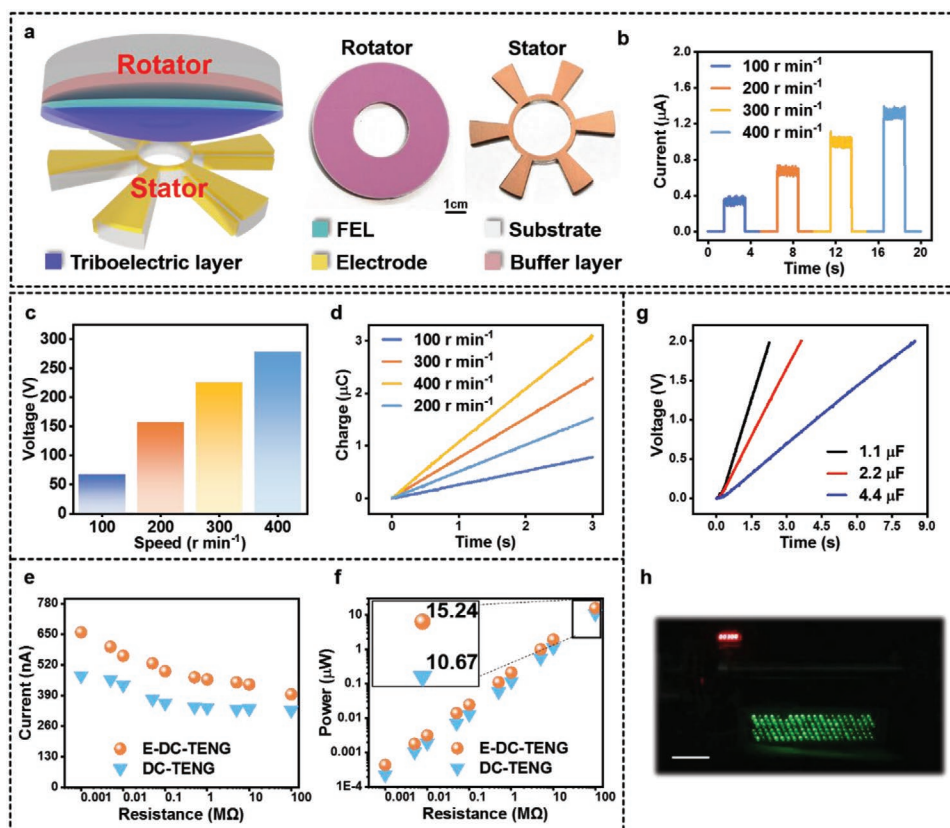
Figure 3. Output performance of sliding mode E-DC-TENG. a) Representative diagram of sliding mode E-DC-TENG. b) Transfer charge and c) peak of I_{sc} and d) V_{oc} outputs of E-DC-TENG at different accelerations. e) Instantaneous peak current and f) power of conventional DC-TENG and E-DC-TENG with various resistances. Inset shows the magnification of power. g) Measured voltage of a capacitor (30 nF) charged by a sliding mode E-DC-TENG.

largely related to the sliding area of the CCE. In other words, it is positively related to the area drawn by the CCE; here, we set the displacement of the device to a constant value of 2 cm. The value of I_{sc} depends mainly on two factors: the quantity of transferred charges and the rate of the charge transfer. As the acceleration increases, the rate of charge transfer increases, and thus I_{sc} also increases. Figure 3d shows the corresponding V_{oc} of the E-DC-TENG at various accelerations with a nearly constant value of ≈50 V. Compared with the performance of the conventional DC-TENG in Figure S4d–f, Supporting Information, it exhibits an obvious enhancement. In addition, the peak current and power of the E-DC-TENG are as shown in Figures 3e,f. The value of I_{sc} maintains almost no decay with an increase in load resistance from 0.001 to 100 MΩ, and the output power naturally increases linearly, reaching 1.84 μW of E-DC-TENG and 0.95 μW of a conventional DC-TENG when the load resistance is 100 MΩ. The enhanced output performance can be demonstrated by a comparative experiment for charging a 30 nF ceramic capacitor to 5 V, and the E-DC-TENG requires less time than a conventional DC-TENG without the use of a rectifier (Figure 3g).

2.4. Output Performance of Rotary Mode E-DC-TENG

To realize a constant output current, we designed a rotary mode E-DC-TENG, a device model diagram and photograph of which

are shown in **Figure 4**a. The equipment used for the experiments is shown in Figure S5, Supporting Information. The rotary-mode E-DC-TENG comprises a stator and rotator. In the rotator, the four layers from top to bottom are acrylic used as a substrate layer, foam applied as the buffer layer, pre-charged PTFE as the FEL, and PTFE as the friction layer. The stator is mainly made of an acrylic substrate, six FEs, and six CCEs in parallel mode. For the rotary-mode E-DC-TENG, a gap d also exists between the FE and CCE, which is the same as that in the sliding-mode E-DC-TENG. A servo motor was used to realize the rotary motion. The output performance of the conventional rotary-mode DC-TENG at different rotation speeds is shown in Figure S6a–c, Supporting Information. The output performances of the E-DC-TENG at different rotation speeds are shown in Figures 4b–d, namely, I_{sc}, V_{oc}, and the transferred charges, respectively. As the rotation speed increases, I_{sc}, V_{oc}, and the transferred charges all increase almost linearly. Moreover, we can also improve the output performance in other ways, such as by increasing the number of CCEs in the array or enlarging the length of the CCE to reach a larger sliding area. It is worth noting that the rotary mode E-DC-TENG has nearly constant output current characteristics, which is suitable for directly driving the microelectronics. To further explore its unique properties for practical applications, we measured the output power of the rotary-mode E-DC-TENG at different loads,

ADVANCED
SCIENCE NEWS
www.advancedsciencenews.com

ADVANCED
MATERIALS
TECHNOLOGIES
www.advmattechnol.de

Figure 4. Output performance of rotary mode E-DC-TENG. a) Representative diagram of rotary mode E-DC-TENG, scale bar = 5 cm. b) I_{sc}, c) V_{oc} output, and d) transfer charge of E-DC-TENG at different rotation rates. e) Instantaneous peak current and f) power of conventional rotary mode DC-TENG and E-DC-TENG with various resistances. g) Measured voltage of a capacitor (1.1, 2.2, and 4.4 µF) charged by a rotary mode E-DC-TENG at 300 r min^{-1}. h) LED array powered by a rotary E-DC-TENG at 300 r min^{-1}. Scale bar = 5 cm.

as shown in Figures 4e,f. In addition, I_{sc} decreases slightly with an increase in the load resistance. Furthermore, we also used the rotary-mode E-DC-TENG to directly charge the various capacitors, and the corresponding voltage curves are as shown in Figure 4g, and the charging capacity curve of the conventional DC-TENG is as shown in Figure S6d, Supporting Information. A light-emitting diode (LED) bulb array can be directly lighted without flashing, as shown in Figure 4h, showing significant potential for mechanical energy harvesting and miniaturization of self-powered systems (Movie S1, Supporting Information).

3. Conclusions

In summary, an E-DC-TENG was designed to improve the breakdown efficiency η to enhance the output performance of the DC-TENG under atmospheric conditions by utilizing the field-enhancing breakdown effect. A specific model and theoretical simulation results were proposed to verify the rationality of this method in principle, and the effectiveness of optimizing the breakdown efficiency η of the DC-TENG was also demonstrated. In the sliding E-DC-TENG, a double enhancement of the transferred charges, I_{sc} and V_{oc}, was achieved. Furthermore, a rotary E-DC-TENG was fabricated for practical applications, and a nearly constant output current was obtained. The output

performance of the E-DC-TENG may be further enhanced using a better electret material with more pre-modulated charges. In this study, not only was a parameter introduced to evaluate the output performance of the DC-TENG, that is, the breakdown efficiency, a simple, effective, and universal method was also provided to optimize the breakdown efficiency.

4. Experimental Section

Fabrication of the Sliding E-DC-TENG: Electric FEL: i) Cut a rectangle-shaped acrylic sheet with dimensions of 4 cm × 10 cm as the substrate by a laser cutter (PLS6.75, Universal Laser Systems) and take a piece of foam attaching to the upper surface of the substrate. Above the foam, a piece of PTFE film with the dimensions of 4 cm × 10 cm × 80 µm as the electric FEL. ii) Cut another acrylic sheet with dimensions of 2 cm × 2 cm as the substrate and take a piece of copper film with the same size and thickness of 64 µm as the FE. iii) The surface charges on the electric FEL are pre-fabricated by surface modulation method.

Slider: Cut a rectangle-shaped acrylic sheet as the substrate with dimensions of 20 mm × 20 mm × 3 mm as the substrate, take a piece of copper tape with thickness of 64 µm attaching to one side of the substrate and cut its lower surface flush with the lower surface of the substrate with a knife as the CCE, and take another copper tape attaching to the bottom surface of the substrate as the FE. There will be a 64 µm height difference between CCE and the dielectric layer. Stator: Take a piece of PTFE film with the dimensions of 4 cm × 10 cm and thickness of 80 µm then attaching it on the upper surface of the electric FEL.

**ADVANCED
SCIENCE NEWS**

www.advancedsciencenews.com

**ADVANCED
MATERIALS
TECHNOLOGIES**

www.advmattechnol.de

Fabrication of the Rotary E-DC-TENG: Electric FEL: i) Cut an annulus-shaped acrylic sheet as the substrate with an inner diameter of 26 mm and an outer diameter of 66 mm and a thickness of 3 mm as the substrate by a laser cutter (PLS6.75, Universal Laser Systems). Then take a piece of foam attaching to the upper surface of the substrate. Above the foam, a piece of PTFE film with the same size and thickness of 80 µm as the electric FEL. ii) Cut another annulus-shaped acrylic sheet as the substrate with an inner diameter of 26 mm and an outer diameter of 66 mm and a thickness of 3 mm, then take a piece of copper film with the same size and thickness of 64 µm as the electrification material. iii) The surface charges on the electric FEL are pre-fabricated by surface modulation method. Stator: i) Cut an annulus-shaped acrylic sheet as the substrate with an inner diameter of 26 mm and an outer diameter of 66 mm and a thickness of 3 mm as the substrate by a laser cutter (PLS6.75, Universal Laser Systems). ii) Cut it further into a sector arrangement with a central angle of 20° and the number of 6 by a laser cutter (PLS6.75, Universal Laser Systems). iii) Take a piece of copper tape with the same size and thickness of 64 µm attaching to the bottom surface of the substrate. Rotator: i) Take a piece of PTFE film with the same size as the substrate and thickness of 80 µm then attaching it on the upper surface of the electric FEL.

COMSOL Simulation of TENG: The 2D potential and electric field distribution between the CCE and charged PTFE films were calculated using the commercial software COMSOL. The distance between the CCE and PTFE layer was set to be 0.07 mm. The surface charge density of each PTFE film was 50 µC m^{-2}.

Measurement and Characterization: The sliding E-DC-TENG was driven by a linear motor (TSMV120-1S). The rotary E-DC-TENG was performed by a rotary motor (80BL165S75-3130TK0). The I_{sc}, V_{oc}, and transferred charges of the E-DC-TENG, and the charging/discharging curves of the direct charging system were measured by a programmable electrometer (Keithley model 6514). The capacitance of the capacitor was tested by a potentiostat (Logic, VSP-300, France).

Supporting Information

Supporting Information is available from the Wiley Online Library or from the author.

Conflict of Interest

The authors declare no conflict of interest.

Data Availability Statement

Research data are not shared.

[1] F.-R. Fan, Z.-Q. Tian, Z. L. Wang, *Nano Energy* **2012**, *1*, 328.

[2] H. Zou, Y. Zhang, L. Guo, P. Wang, X. He, G. Dai, H. Zheng, C. Chen, A. C. Wang, C. Xu, Z. L. Wang, *Nat. Commun.* **2019**, *10*, 1427.

[3] G. Zhu, J. Chen, T. Zhang, Q. Jing, Z. L. Wang, *Nat. Commun.* **2014**, *5*, 3426.

[4] L. Zhou, D. Liu, J. Wang, Z. L. Wang, *Friction* **2020**, *8*, 481.

[5] Y. Liu, W. Liu, Z. Wang, W. He, Q. Tang, Y. Xi, X. Wang, H. Guo, C. Hu, *Nat. Commun.* **2020**, *11*, 1599.

[6] W. He, W. Liu, J. Chen, Z. Wang, Y. Liu, X. Pu, H. Yang, Q. Tang, H. Yang, H. Guo, C. Hu, *Nat. Commun.* **2020**, *11*, 4277.

[7] J. Chung, D. Heo, G. Shin, D. Choi, K. Choi, D. Kim, S. Lee, *Adv. Energy Mater.* **2019**, *9*, 1901731.

[8] Z. Wang, W. Liu, W. He, H. Guo, L. Long, Y. Xi, X. Wang, A. Liu, C. Hu, *Joule* **2021**, *5*, P441.

[9] F. Xi, Y. Pang, W. Li, T. Jiang, L. Zhang, T. Guo, G. Liu, C. Zhang, Z. L. Wang, *Nano Energy* **2017**, *37*, 168.

[10] J. Wang, Z. Wu, L. Pan, R. Gao, B. Zhang, L. Yang, H. Guo, R. Liao, Z. L. Wang, *ACS Nano* **2019**, *13*, 2587.

[11] C. Zhang, T. Zhou, W. Tang, C. Han, L. Zhang, Z. L. Wang, *Adv. Energy Mater.* **2014**, *4*, 1301798.

[12] X. Li, X. Yin, Z. Zhao, L. Zhou, D. Liu, C. Zhang, C. Zhang, W. Zhang, S. Li, J. Wang, Z. L. Wang, *Adv. Energy Mater.* **2020**, *10*, 1903024.

[13] H. Ryu, J. H. Lee, U. Khan, S. S. Kwak, R. Hinchet, S.-W. Kim, *Energy Environ. Sci.* **2018**, *11*, 2057.

[14] T. Kim, D. Y. Kim, J. Yun, B. Kim, S. H. Lee, D. Kim, S. Lee, *Nano Energy* **2018**, *52*, 95.

[15] J. Wang, Y. Li, Z. Xie, Y. Xu, J. Zhou, T. Cheng, H. Zhao, Z. L. Wang, *Adv. Energy Mater.* **2020**, *10*, 1904227.

[16] H. Shao, J. Fang, H. Wang, L. Dai, T. Lin, *Adv. Mater.* **2016**, *28*, 1461.

[17] J. Liu, A. Goswami, K. Jiang, F. Khan, S. Kim, R. McGee, Z. Li, Z. Hu, J. Lee, T. Thundat, *Nat. Nanotechnol.* **2018**, *13*, 112.

[18] J. Liu, F. Liu, R. Bao, K. Jiang, F. Khan, Z. Li, H. Peng, J. Chen, A. Alodhayb, T. Thundat, *ACS Appl. Mater. Interfaces* **2019**, *11*, 35404.

[19] R. Xu, Q. Zhang, J. Y. Wang, D. Liu, J. Wang, Z. L. Wang, *Nano Energy* **2019**, *66*, 2211.

[20] Q. Zhang, R. Xu, W. Cai, *Nano Energy* **2018**, *51*, 698.

[21] Y. Yang, H. Zhang, Z. L. Wang, *Adv. Funct. Mater.* **2014**, *24*, 3745.

[22] J. Luo, L. Xu, W. Tang, T. Jiang, F. R. Fan, Y. Pang, L. Chen, Y. Zhang, Z. L. Wang, *Adv. Energy Mater.* **2018**, *8*, 1800889.

[23] H. J. Yoon, M. Kang, W. Seung, S. S. Kwak, J. Kim, H. T. Kim, S. W. Kim, *Adv. Energy Mater.* **2020**, *10*, 2000730.

[24] D. Liu, X. Yin, H. Y. Guo, L. L. Zhou, X. Y. Li, C. L. Zhang, J. Wang, Z. L. Wang, *Sci. Adv.* **2019**, *5*, eaav6437.

[25] C. Chen, H. Guo, L. Chen, Y. C. Wang, X. Pu, W. Yu, F. Wang, Z. Du, Z. L. Wang, *ACS Nano* **2020**, *14*, 4585.

[26] S. Li, D. Liu, Z. Zhao, L. Zhou, X. Yin, X. Li, Y. Gao, C. Zhang, Q. Zhang, J. W. Z. L. Wang, *ACS Nano* **2020**, *14*, 2475.

[27] X. Yin, D. Liu, L. Zhou, X. Li, G. Xu, L. Liu, S. Li, C. Zhang, J. Wang, Z. L. Wang, *Adv. Funct. Mater.* **2020**, *30*, 2002547.

[28] L. Zhou, D. Liu, S. Li, Z. Zhao, C. Zhang, X. Yin, L. Liu, S. Cui, Z. L. Wang, J. Wang, *Adv. Energy Mater.* **2020**, *10*, 2000965.

[29] Z. Zhao, Y. Dai, D. Liu, L. Zhou, S. Li, Z. L. Wang, J. Wang, *Nat. Commun.* **2020**, *11*, 6186.

[30] Z. Yi, D. Liu, L. Zhou, S. Li, Z. Zhao, X. Li, Z. L. Wang, J. Wang, *Nano Energy* **2021**, *84*, 105864.

[31] D. Liu, L. Zhou, S. Li, Z. Zhao, X. Yin, Z. Yi, C. Zhang, X. Li, J. Wang, Z. L. Wang, *Adv. Mater. Technol.* **2020**, *5*, 2000289.

[32] D. Liu, L. Zhou, Z. L. Wang, J. Wang, *iScience* **2021**, *24*, 102018.

[33] Z. L. Wang, A. C. Wang, *Mater. Today* **2019**, *30*, 34.